Microfluid Nanofluid (2009) 7:519–530
DOI 10.1007/s10404-009-0410-0

RESEARCH PAPER

Analysis of capillary filling in nanochannels with electroviscous effects

Vinh-Nguyen Phan · Chun Yang · Nam-Trung Nguyen

Received: 5 November 2008 / Accepted: 1 January 2009 / Published online: 29 January 2009

Abstract Capillary filling is the key phenomenon in planar chromatography techniques such as paper chromatography and thin layer chromatography. Recent advances in micro/nanotechnologies allow the fabrication of nanoscale structures that can replace the traditional stationary phases such as paper, silica gel, alumina, or cellulose. Thus, understanding capillary filling in a nanochannel helps to advance the development of planar chromatography based on fabricated nanochannels. This paper reports an analysis of the capillary filling process in a nanochannel with consideration of electroviscous effect. In larger scale channels, where the thickness of electrical double layer (EDL) is much smaller than the characteristic length, the formation of the EDL plays an insignificant role in fluid flow. However, in nanochannels, where the EDL thickness is comparable to the characteristic length, its formation contributes to the increase in apparent viscosity of the flow. The results show that the filling process follows the Washburn's equation, where the filled column is proportional to the square root of time, but with a higher apparent viscosity. It is shown that the electroviscous effect is most significant if the ratio between the channel height (h) and the Debye length (κ^{-1}) reaches an optimum value (i.e. $\kappa h \approx 4$). The apparent viscosity is higher with higher zeta potential and lower ion mobility.

Keywords Nanofluidics · Nanochannel · Capillary filling · Apparent viscosity · Planar chromatography

V.-N. Phan · C. Yang · N.-T. Nguyen (✉)
School of Mechanical and Aerospace Engineering, Nanyang Technological University, 50 Nanyang Avenue, Singapore 639798, Singapore
e-mail: mntnguyen@ntu.edu.sg

List of symbols

A_c	Cross-section of the channel
A, B, C, D, E	Reduced variables
e	Elementary charge, 1.305×10^{-19}C
E_s	Streaming electric field strength
F_e	Electrical force
F_s	Surface force
F_v	Viscous drag force
h	Channel's height
I_c	Conduction current
I_s	Streaming current
k	Boltzmann's constant, 1.381×10^{-23} JK^{-1}
n	Local concentration
n^0	Bulk concentration
q_a	Accumulated charge
T	Room temperature
t	Time variable
u	Fluid velocity
U_s	Streaming potential
w	Channel's width
x	Capillary filling length
y	Coordinate across the channel height
z	Charge number
EDL	Electric double layer
IC	Initial condition
ODE	Ordinary differential equation
$\bar{}$	Average value across the height
$\hat{}$	Divide by channel width w
$_i$	Belong to ion species i

Greek symbols

α, β, γ	Functions in phase space
ε	Relative permittivity of the fluid

ε_0	Permittivity of free space 8.854×10^{-12} CV^{-1} m^{-1}
ζ	Zeta potential
θ	Contact angle
η	Material dimensionless parameter
κ	Inverse of Debye thickness
λ	Conductivity of the fluid/eigenvalue in Appendix 1
Λ_m	Molar conductivity of solution
μ	Dynamic viscosity
μ_a	Apparent dynamic viscosity
$\Delta\mu$	Increase in dynamic viscosity
υ	Ion mobility
ξ	Auxiliary variable
ρ_m	Mass density of the fluid
ρ_q	Charge density
σ	Surface tension
χ	Auxiliary variable
Ψ	Electrostatic potential across the channel's height
$\tilde{\Psi}$	Normalized electrostatic potential $\tilde{\Psi} = \frac{e\Psi}{kT}$

1 Introduction

With the advantages of low cost, speed, and simplicity, planar chromatography is an important technique for analytical chemistry. Theories, techniques, and applications of planar chromatography have been reported in the literature (Sherma 2002, 2004, 2006, 2008). Traditionally, this technique is based on capillary filling phenomenon to drive a mobile phase through a porous material, such as paper, silica gel, alumina, or cellulose, which serves as stationary phase. Difference in affinities leads to the separation of the analytes. Since recent years, advances in micro/nanotechnologies allow for the fabrication of structures at nanoscale (i.e. from several to hundreds of nanometers) (Eijkel and van den Berg 2005; Mijatovic et al. 2005; Perry and Kandlikar 2006; Yuan et al. 2007). These technological advances promise the replacement of traditional stationary phase in planar chromatography by more deterministic, controllable nanostructures, such as nanochannels. Therefore, understanding capillary filling in nanochannel can contribute to the further development of planar chromatography.

The coupling of electrokinetic and hydrodynamic phenomena was first observed at the beginning of the nineteenth century by Reuss (1809) and was first theoretically explained by Helmholtz and Smoluchowski (Smoluchowski 1903) based on simple description on the electric double layer. Washburn (1921) provided a simple formula to describe capillary filling in a porous material. The formula states that the filling distance is proportional to square root of time. Theoretical and experimental studies on capillary filling in nanochannels have been performed in recent years. In 1923, Debye and Hückel (1923) proposed a model in which the ionic distribution in solutions follows Boltzmann energy distribution. A direct result of this model is the ionic distribution and electric potential distribution in capillary channel as determined by Poisson–Boltzmann (PB) equation. This PB equation can be solved analytically for the case of single flat EDL (Hunter 1981; Russel et al. 1989; Verwey and Overbeek 1948). Utilizing this feature, thin EDL approximation can be used to find the ionic distribution in almost all capillary channel geometry, as long as the EDL is thin enough in comparison to the characteristic dimension (Burgreen and Nakache 1964). Another approximation which is usually useful is the low potential approximation, which linearizes the PB equation and therefore makes it, theoretically, solvable for any boundary condition. In 1948, Verwey and Overbeek derived the solution for the case of plane parallel slit-shaped channel using low potential approximation (Verwey and Overbeek 1948). Analytic solutions for special cases were also studied. Burgreen and Nakache (1964) introduced exact solution for PB equation for the case of parallel slit-shaped channel in term of elliptic integral. Although the numerical value of the elliptic integral can be calculated quite easily nowadays using computer, Burgreen and Nakache's result is difficult to use for further analytic investigation. In 1965, Rice and Whitehead (1965) suggested a solution for PB equation in cylindrical channel using low potential approximation. The result was expressed in term of Bessel's functions. Electroviscous effect for electroosmotic flow was also presented. In 1974, Levine and Neale (1974) investigated the electrophoresis problem of a swarm of identical, dielectric, spherical particles, with consideration of the interaction of individual particles through the associated electric field. The result justified Smoluchowski's model for electrophoretic flow with in porous media.Recognizing the practical limitation in Rice and Whitehead's result, which require low ζ potential, in 1975, Levine et al. (1975a) published a modification model that is more suitable for higher ζ potential. However, this is also an approximated model because it uses a mathematical approximation proposed by Philip and Wooding (1970). Also in 1975, Levine et al. (1975b), utilizing series expansion, improved the result found previously by Burgreen and Nakache. The electroviscous effect in electroosmotic flow was also discussed. As a contribution to membrane separation technology, in 1995, Bowen and Jenner (Bowen and Jenner 1995) introduced a cell model for charged colloidal dispersion. The model considered the effect of interparticle, including London-van der Waals, electroviscous, and hydration forces. Numerical method was used to solve the non-linear PB equation. In 1997, Yang and Li (1997) analyzed pressured driven flow in a rectangular microchannel, with

consideration of electroviscous effect. Numerical method was used to solve the P–B equation. The result showed a reduction in flow rate, which is a result of electroviscous force. In 2002, Hsu et al. (2002) gave a theoreticalinvestigation on the electrokinetic flow of an electrolyte solution through an elliptical microchannel. Three kinds of boundary condition for PB equation, including constant surface charge, constant surface potential and charge-regulated surface were considered. Numerical method was used to solve the governing equations. The results showed that for a constant cross-sectional area, the volumetric flow rate and the streaming potential increase with an increase in the aspect ratio while total electric current and the electroviscous effect may exhibit a local minimum as the aspect ratio varies. In 2005, Ren and Li (2005) introduced an improvement on the electrokinetic flow in microchannel. The authors showed that traditional understanding about Boltzmann distribution of ion in the channel may not be sufficient in some cases, such as dilute solution or very small channel. Improved model with consideration of the dissociation constants of substances show remarkable reduction in flow rate in comparison to conventional solutions, even for a large channel such as microchannel. Mohiuddin Mala and Li (1999) performed an experimental investigation on the pressure-driven water flow through microtubes with diameters ranging from 50 to 254 μm. It was found that for a relatively high flow rate, the required pressure gradient to force the liquid through the microtube is higher than theoretically predicted; however, for small flow rate, theoretical and experimental data agree well. In 2007, Huang and Yang (2007) presented the ionic concentration variation in overlapped EDL that lead to changing in electrokinetic behavior in comparison to that predicted by traditional theory. Modified concentration approach was introduced to solve the PB equation. Numerical result obtained showed that the constant surface charge assumption is more suitable to use in low-salt regime. Also Huang and Yang (2008) presented the effect of ion depletion and enrichment zone in capillary channel to the dynamics of fluid. Ion depletion/enrichment zone were created by external electric field. Experimental results showed that the low conductivity within the depletion zone induces a rapid electroosmotic flow, which in turn prompts the generation of vortex flow structures within the depletion zone. Tas et al. (2003) found that water plugs in hydrophilic nanochannels can generate a significant negative pressure due to high-tensile capillary force. Tas et al. (2004) investigated the capillary filling speed of water and sodium chloride (NaCl) in nanochannels with rectangular cross section and a height of 100 nm. The experimental results showed that the filling distance versus time follows Washburn's model, but the filling speed is lower than expected. Lyklema et al. (2005) in his book explained the formation of electrical double layer (EDL) is due to the non-electric affinity of charge-determining ions for a surface such as dissociation or adsorption of charged molecules from the solution. Han et al. (2006) investigated the filling kinetics of different liquids in nanofabricated capillaries with rectangular cross-section. Their results confirmed Washburn's model in capillary filling. The trapping of air bubbles during filling process was observed. The authors suggested that nanochannels should be used as an idealized model to study mass transport mechanisms in systems where surface phenomena dominate. Huang et al. (2006) reported on theoretical and numerical investigations on capillary flow inside microchannels with patterned surfaces. The equivalent contact angle (ECA) model for flows with small capillary number was introduced and was confirmed by numerical results. Van Honschoten et al. (2007) suggested a model of elastocapillary filling in deformable channels. During the filling process, nanochannels are easily deformed due to the high negative pressure across the meniscus. It is shown in their model that in the elastocapillary filling process, two opposite effects compete: decrease in the channel cross section increases the flow resistance, while the Laplace pressure that acts as the driving force becomes more negative due to an increase in the meniscus curvature. It was also concluded that the filling speed qualitatively follows Washburn's relation. Mortensen et al. (2006, 2007 reported on an investigation on the linear-response theory for the mass and charge transport coefficients that satisfy Onsager relations. Hilbert space eigenfunction expansion was used to derive the results. Mortensen and Kristensen (2008) theoretically investigated the electroviscous effect of capillary filling in nanochannels. The theory was established based on a linear relationship among liquid flow rate, electric current, pressure drop and voltage drop. It was found that the apparent viscosity reaches a maximum in the mesoscopic regime where the hydraulic radius is comparable to the Debye screening length. However, comparison between theory and experimental data showed that electroviscous effect contributes only a portion of the overall increase in viscosity. This suggested that other phenomena may be involved in the change of viscosity during capillary filling process in nanochannels. In 2008, Chakraborty (2008a, b) developed a model to describe the complex coupling phenomena between electrohydrodynamic effects and other transport characteristic in the narrow confinement, such as interfacial wettability. One of the important results is that the hydrophobic interaction may lead to an amplification of the ζ potential. Petsev (2008) gave a review about transport effects in nanochannels, including electroosmosis, electrophoretic, and pressure driven flow. The review presented the physics behind fluidic transport in nanochannels, especially about the effect of Debye layer.

Nanochannels for capillary filling experiments were fabricated in a wide range of materials. Jeong et al. (2007) reported on a simple method using hydrophilic poly(ethylene glycol) (PEG) to fabricate nanochannels. The capillary filling experiment was performed in PEG-based microchannels to compare with those made in hydrophobic polydimethylsiloxane (PDMS). The results agreed well with the theoretical predictions based on the simple Poiseuille formation. Lerch and Jacobson (2007) presented microfluidic device designs with a two-dimensional planar format and methods to facilitate efficient sample transport along both dimensions. The experiment illustrated fluid handling capabilities in a microfluidic device with a planar format. Persson et al. (2007) reported on the fabrication of SiO_2 nanochannels using the so-called double thermal oxidation scheme. The nanochannels have heights ranging from 14 to 300 nm and widths of 2.5, 5 and 10 μm. Capillary filling experiments were also performed to test the channels. Data of the apparent viscosities for various substances and channel heights were reported. Thamdrup et al. (2007) observed the formation of bubbles during capillary filling. The experiments were performed with water in SiO_2 nanochannels with heights ranging from 33 to 158 nm. It was found that the formation of an isolated pinned bubble causes a short-time reduction of the filling speed and is accompanied by a forward jump of the meniscus. Van Delft et al. (2007) introduced a microfabricated Fabry-Pèrot interferometer with nanochannels of various heights between 6 and 20 nm embedded in its cavity. The device allows the investigation of fluid behaviors inside a nanochannel without using fluorescent substances. Capillary filling experiments were carried out in these channels and revealed that the entrapment of air bubbles may happen during the filling process. Zimmermann et al. (2007) designed a capillary pump for autonomous capillary systems, comprising microstructures of various shapes with dimensions from 15 to 250 μm. The pumps were designed to have a small flow resistance and are preceded by a constricted microchannel, which acts as a flow resistance. The authors also showed how to connect different pumps with different specifications to achieve the desired purpose. Tas et al. (2008) presented a procedure for fabrication of silicon-based nanochannels with heights ranging from 5 to 50 nm using a thin silicon oxide spacer layer. Capillary filling experiments were carried out in these channels. The results showed that the filling process in 5-nm-height channels agrees with Washburn's model but with a Washburn's coefficient 1.6 times lower than expected.

When the size of the channel decreases to nanoscale, surface effects become more significant. The electrokinetic force, which may be negligible in larger scale channels now contributes significantly to the dynamics of the fluid column inside the nanochannel. It is shown in literature that most of current theories on the electroviscouseffec in capillary filling are based on the similarity between capillary filling and pressure-driven flow, which neglect the continuous absorption of ions at the meniscus, a special phenomenon of capillary filling.This paper reports an analysis for capillary filling in nanochannels with consideration of electroviscous effects. The presented model describes charge distribution within the channel and evaluates the interactions between electrokinetic effects and surface force as well as viscous force. The model is used to estimate the contribution of electroviscous effects on the increase in apparent viscosity. Figure 2 compares the two main current theories on the increase in apparent viscosity in nanochannels with the new description of capillary filling in nanochannels presented in this paper.

2 Analytical model for capillary filling in a nano-channel

2.1 Physical description

Figure 1 describes the geometry for the model of capillary filling in a nanochannel with a height of h and a width w. The channel is of high aspect ratio $w/h \gg 1$ and can be considered as two parallel plates. The channel wall is positive charged. The shade areas in Fig. 1 represent the electrical double layer (EDL), containing the compact layer attached to the channel wall and the mobile layer. When liquid fluid flows along the nanochannel, the absorption of positive charge into the wall causes negative ions to accumulate at the meniscus. Charge imbalance between the meniscus area and the channel inlet induces a streaming voltage. This streaming voltage generates a conductive current.

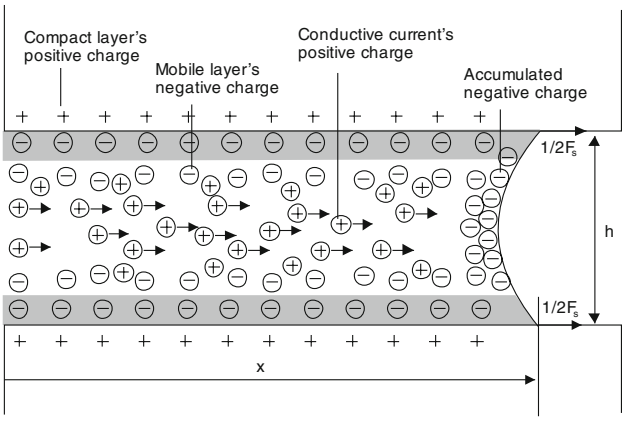

Fig. 1 Capillary filling in a nanochannel: Ion distribution and movement inside a liquid column moving in a nanochannel due to capillary filling

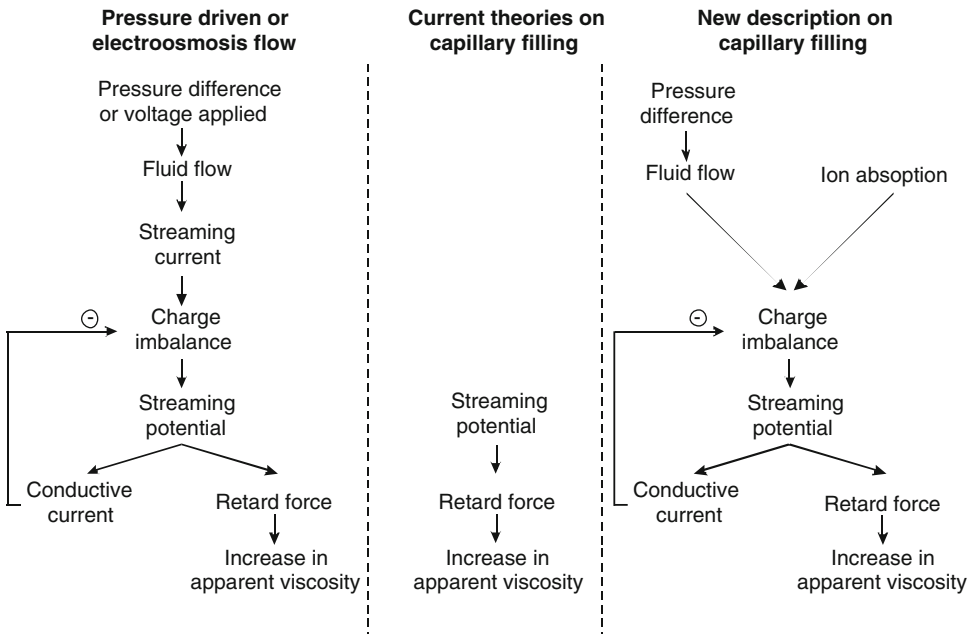

Fig. 2 Comparison of existing theoretical approaches for analyzing the increase in apparent viscosity and the present analysis on capillary filling

2.2 Mathematical formulations

The capillary filling phenomenon in a nanochannel is assumed to be governed by the following physics and assumptions.

2.2.1 Continuum assumption

The Knudsen number, *Kn* represents the ratio of the molecular mean-free path to the characteristic length. In order to apply continuum assumption, low Knudsen number is required (Nguyen 2008). For most of liquids, the mean-free path is in the order of few nanometers. Thus, even in nanochannels with a height from tens to several hundreds nanometers, the continuum assumption ($kn < 10^{-1}$) is still valid.

2.2.2 Electrokinetic flow

The driving force depends on the surface tension of the fluid and the contact angle between the fluid and the channel wall. Due to the surface tension at the meniscus, a static pressure difference builds up between the channel entrance and the meniscus, resulting in a capillary filling flow. With the continuum assumption, the flow in the nanochannel has the typical parabolic velocity profile. When the liquid fills the nanochannel, the zeta potential ζ of the channel causes the redistributions of ions to form the channel electric double layer (EDL) (Debye and Hückel 1923; Smoluchowski 1903), as shown in Fig. 1. If the channel wall is positive charged, it induces apparent accumulation of negative charge ions in the meniscus region. The total electric charge in this region, termed as the accumulated charge q_a, creates an electric field E_S that in turn generates a conductive current. Voltage drop along this electric field is the streaming voltage U_S. The charge balance considers the total charge of the liquid column, the total charge on the channel's wall, the accumulated charge, the streaming current and the conductive current. The charge density distribution in the nanochannel is governed by the Poisson-Boltzmann (PB) equation. For low zeta potential ζ, the Debye-Hückel approximation can be used to linearize the PB equation.

Electrostatic interaction between the induced streaming potential and the charge density of the liquid column slows down the capillary filling effect. Electrostatic interaction is governed by Gauss's theorem and Lorentz's force law. The effect of all the aforementioned forces on the dynamics of the fluid column is governed by Newton's second law.

2.2.3 Capillary force

The pressure difference across the meniscus of the moving liquid column is assumed by the Young-Laplace equation:

$$\Delta p = \sigma\left(\frac{1}{r_1} + \frac{1}{r_2}\right) \tag{1}$$

where Δp is the pressure difference, σ is the surface tension, and r_1 and r_2 are the radii of curvature. Figure 1 shows the forces acting on the meniscus. Assuming $w \gg h$, the capillary force can be described as

$$F_S = 2\sigma w \cos\theta \tag{2}$$

where F_S is the force at the contact line caused by surface tension, and θ is the contact angle between the fluid and the surface's wall. In this investigation, the variation of surface

energy due to accumulation of charged particles near the meniscus, as described in Gibbs–Duhem equation, is neglected. It was reported in literature that the liquid slip at the solid–liquid interface (Yang et al. 2004) and interaction with electrokinetic effect (Chakraborty and Chakraborty 2008) may lead to modification of effective contact angle. However, in capillary filling in nanochannel, the shear stress and streaming voltage diminish fast. In such condition; the modification in effective contact angle is negligible.

2.2.4 Viscous force

Capillary filling flow can be considered as a pressure-driven flow, except the fact that the velocity at the meniscus has a plug distribution. Similar to the entrance effect in microscale, at the exit region, the velocity changes from its parabolic profile to the plug-like profile. This entrance effect is important at the initial stage of filling process, especially when the filling length is comparable to the entrance length. The entrance effect introduces additional flow resistance. This phenomenon has been carefully discussed in recent investigation (Chakraborty 2007; Chakraborty and Mittal 2007; Huang et al. 2001; Chakraborty 2005). However, when the filling length is much longer than the entrance length, the important of entrance effect diminishes. In this investigation, because the asymptotic solution is considered, the entrance effect is assumed to be negligible due to the low Reynolds number here. The velocity profile of 1D laminar pressure-driven flow between two infinite parallel plates is given by (Kundu and Cohen 1990).

$$u = \bar{u}\left(6\frac{y^2}{h^2} - \frac{3}{2}\right), \quad -\frac{h}{2} < y < \frac{h}{2} \tag{3}$$

where u is the fluid velocity, $\bar{u}$ is the average velocity across the channel height, y is the coordinate across the channel height. The average velocity $\bar{u}$can be proven to be equal to the velocity of the meniscus due to its plug-like velocity distribution. The variable $\bar{u}$ represents both front surface velocity and average velocity across the channel height. With the above assumptions, the viscous force act on the entire liquid column can be determined by

$$F_{\mathrm{V}} = \left(\mu\frac{\mathrm{d}u}{\mathrm{d}y}\bigg|_{y=\frac{h}{2}} - \mu\frac{\mathrm{d}u}{\mathrm{d}y}\bigg|_{y=-\frac{h}{2}}\right)wx = -\frac{12\mu\bar{u}}{h}wx \tag{4}$$

where F_{V} is the viscosity force acting on the fluid and μ is the dynamic viscosity of the fluid.

2.2.5 EDL charge density distribution

The charge density distribution determines the electrostatic force in the capillary filling process. In a nanochannel, the potential distribution and consequently the charge density distribution is governed by the Poisson–Boltzmann equation (Debye and Hückel 1923; Petsev 2008). Because the filling length is considered much longer than the channel height, it is appropriate to assume that the potential and charge density distribution across the channel is influenced by the ζ potential only and not by the streaming potential.

$$\nabla^2\Psi = -\frac{\rho_q}{\varepsilon\varepsilon_0} = -\frac{e}{\varepsilon\varepsilon_0}\sum_i z_i n_i^0 \exp\left(-\frac{z_i e\Psi}{kT}\right) \tag{5}$$

where Ψ is the electrostatic potential, ρ_{q} is the charge density, $e = 1.6021 \times 10^{-19}\mathrm{C}$ is the elementary charge, ε is the relative permittivity of the fluid, $\varepsilon_0 = 8.854 \times 10^{-12}\ \mathrm{CV^{-1}\ m^{-1}}$ is the permittivity of vacuum, z_i is the charge number of ionic species i, n_i^0 is the bulk concentration of ionic species i, $k = 1.381 \times 10^{-23}\mathrm{JK^{-1}}$ is Boltzmann's constant, and T is the temperature. For a symmetric binary electrolyte (i.e. $z_1 = z_2 = z_3$), Eq. (5) can be written as

$$\nabla^2\tilde{\Psi} = \frac{\kappa^2}{z}\sin\mathrm{h}(z\tilde{\Psi}) \tag{6}$$

where $\tilde{\Psi} = e\Psi/kT$ is the dimensionless potential, and κ is the Debye parameter, $\kappa^2 = 2e^2z^2n^0/\varepsilon\varepsilon_0 kT$ (n^0 is the bulk concentration of the solute). With the Debye–Hückel approximation of a low potential, Eq. (6) can be linearized to

$$\nabla^2\tilde{\Psi} = \kappa^2\tilde{\Psi} \tag{7}$$

which solution is given by (Petsev 2008).

$$\tilde{\Psi}(y) = \frac{e\zeta}{kT}\frac{\cos\mathrm{h}(-\kappa y)}{\cos\mathrm{h}(\kappa h/2)} \tag{8}$$

Therefore

$$\Psi(y) = \zeta\frac{\cos\mathrm{h}(-\kappa y)}{\cos\mathrm{h}(\kappa h/2)} \tag{9}$$

and the charge density distribution is given by

$$\rho_{\mathrm{q}} = -\varepsilon\varepsilon_0\frac{\mathrm{d}^2\Psi}{\mathrm{d}y^2} = -\varepsilon\varepsilon_0\zeta\kappa^2\frac{\cos h(\kappa y)}{\cos h(\kappa h/2)} \tag{10}$$

In order to keep the result simple for further manipulation, the Debye–Hückel of low potential is used here. At room temperature, this approximation is only valid for ζ potential below 26 mV (Conlisk 2005). This restriction theoretically limits the applications of the result. In literature, there were studies describing the solution of PB equations in different conditions, utilizing various approaches (Bowen and Jenner 1995; Burgreen and Nakache 1964; Hsu et al. 2002; Huang and Yang 2007; Hunter 1981; Levine et al. 1975a, b; Levine and Neale 1974; Rice and Whitehead 1965; Russel et al. 1989; Verwey and Overbeek 1948; Yang and Li 1997). Also, Ren and Li (2005) introduced a modification in PB equation for

the case of dilute solution, such that the electroviscous effect becomes more significant, even for microchannel. The approach introduced in this investigation does not restrict the application of those results instead of Eq. (10). However, in such cases, the final result should be much more complicated.

2.2.6 Conductivity of the electrolyte

The conductivity of an electrolyte in a nanochannel can be calculated by Eq. (11):

$$\lambda = \sum_i \lambda_i = \sum_i |z_i| e v_i n_i \tag{11}$$

where λ is the total conductivity of the electrolyte, λ_i is the individual contribution of ionic species i to the conductivity, v_i is the electrical mobility of ionic species i, n_i is the concentration of ionic species i. Substituting Poisson–Boltzmann equation into Eq. (11) gives

$$\lambda = n^0 \sum_i |z_i| e v_i \exp(-z\tilde{\Psi}) \tag{12}$$

Then, the average conductivity across the channel height can be computed from

$$\bar{\lambda} = \frac{1}{h}\int_{-\frac{h}{2}}^{\frac{h}{2}} \lambda \mathrm{d}y = n^0 \frac{1}{h} e \int_{-\frac{h}{2}}^{\frac{h}{2}} \sum_i |z_i| v_i \exp(-z_i\tilde{\Psi}) \mathrm{d}y \tag{13}$$

With the Debye–Hückel approximation, Eq. (13) can be expressed as

$$\bar{\lambda} = n^0 \frac{1}{h} e \int_{-\frac{h}{2}}^{\frac{h}{2}} \sum_i |z_i| v_i (1 - z_i\tilde{\Psi}) \mathrm{d}y \tag{14}$$

If a monovalent electrolyte such as NaCl solution ($z_+ = -z = 1$) is considered, Eq. (14) can be rewritten as

$$\bar{\lambda} = n^0 e (v_+ + v_-) \left(1 + \frac{1}{h} \frac{v_- - v_+}{v_+ + v_-} \int_{-\frac{h}{2}}^{\frac{h}{2}} \tilde{\Psi} \mathrm{d}y \right) \tag{15}$$

Substituting the solution of the potential distribution Eqs. (10) into Eq. (16) and performing the integration result in

$$\bar{\lambda} = n^0 e (v_+ + v_-) \left(1 + \frac{\zeta e}{kT} \frac{v_- - v_+}{v_+ + v_-} \frac{2 \tanh\left(\frac{\kappa h}{2}\right)}{\kappa h} \right) \tag{16}$$

Defining the molar conductivity of a monovalent electrolyte $\Lambda_\mathrm{m} = \sum_i e N_\mathrm{A} v_i$, we can obtain the expression from the average conductivity as

$$\bar{\lambda} = n^0 \frac{\Lambda_\mathrm{m}}{N_\mathrm{A}} \left(1 + \frac{\zeta e}{kT} \frac{v_- - v_+}{v_+ - v_-} \frac{2 \tanh\left(\frac{\kappa h}{2}\right)}{\kappa h} \right) \tag{17}$$

2.2.7 Charge balance

Unlike in pressure-driven flow or electrosomosis flow, where the ion absorption at the channel wall is saturated, in capillary filling, ion absorption takes place continuously during the filling process, creating a charged surface attached to the wall. Due to ion absorption, an accumulated charge exists in the fluid. Because the channel wall far away from the meniscus is quickly saturated, the absorption only takes places near the meniscus. Hence, the charge accumulation is assumed to be at the meniscus only. The speed of development of the charged surface is equal to the meniscus speed, and the net charge in the nanoscale volume must neutralize the surface charge, the contribution of ion absorption to the development of accumulated charge can be expressed by the streaming current I_S

$$I_\mathrm{S} = \int_{A_\mathrm{C}} u \rho_\mathrm{q} \mathrm{d}A = \int_{-\frac{h}{2}}^{\frac{h}{2}} u \rho_\mathrm{q} w \mathrm{d}y \tag{18}$$

The accumulated charge induces streaming current U_S, which in turn causes the conductive current I_C

$$I_\mathrm{C} = -\frac{U_\mathrm{S} \bar{\lambda} A_\mathrm{C}}{x} \tag{19}$$

where $A_\mathrm{C} = wh$ is the cross section of the channel. Let the accumulate charge at the meniscus of the liquid column is q_a, the charge balance for the liquid column requires

$$I_\mathrm{c} + I_\mathrm{s} = \frac{\mathrm{d}}{\mathrm{d}t} q_\mathrm{a} \tag{20}$$

Substituting Eqs. 18 and 19 into Eq. (20) results in the charge balance equation

$$-\frac{U_\mathrm{s} \bar{\lambda} w h}{x} + \int_{-\frac{h}{2}}^{\frac{h}{2}} u \rho_\mathrm{q} w \mathrm{d}y = \frac{\mathrm{d}}{\mathrm{d}t} q_\mathrm{a} \tag{21}$$

It was shown (Chakraborty and Das 2008) that the convective transport of ions under the influence of streaming field is usually ignored in literature, leading to inaccuracy in estimation of streaming potential. In Eq. (21), the streaming current is expressed using the general velocity field u, without explicit relation to the causes of this velocity, hence the mistake is avoided.

2.2.8 Newton's second law

The force balance on the moving liquid column is expressed according to Newton's second law

$$F_\mathrm{S} + F_\mathrm{V} + F_\mathrm{e} = \frac{\mathrm{d}}{\mathrm{d}t} (\rho_\mathrm{m} w h x \bar{u}) \tag{22}$$

where F_e is the electric force due to interaction between the induced streaming potential and the EDL charge density of the channel wall, and ρ_m is the mass density of the fluid. The electric charge accumulated at the front of the fluid column produces an electric field, namely the streaming potential field. Such electric field in turn causes electrostatic force acting on the entire liquid column. Assuming a constant electric field along the channel, the electric force is

$$F_e = -x \int_{A_C} \frac{U_s}{x} \rho_q dA = -xw \int_{-\frac{h}{2}}^{\frac{h}{2}} \frac{U_s}{x} \rho_q dy \tag{23}$$

Applying Gauss's theorem to the meniscus area, where the accumulated charge is located, the streaming electric field strength is

$$-E_s = \frac{U_s}{x} = \frac{q_a}{A_C \varepsilon\varepsilon_0} = \frac{q_a}{wh\varepsilon\varepsilon_0} \tag{24}$$

Substituting Eq. (24) into Eq. (23) gives an expression for the electric force

$$F_e = -\frac{q_a x}{h\varepsilon\varepsilon_0} \int_{-\frac{h}{2}}^{\frac{h}{2}} \rho_q dy \tag{25}$$

Also, substituting Eq. (24) into Eq. (21) results in

$$-\frac{q_a \bar{\lambda}}{\varepsilon\varepsilon_0} + \int_{-\frac{h}{2}}^{\frac{h}{2}} u\rho_q w dy = \frac{d}{dt} q_a \tag{26}$$

The force balance and the charge balance the form the equation system for the capillary filling effect in a nanochannel are expressed as

$$\begin{cases} 2\sigma w \cos\theta - \dfrac{12\mu\bar{u}}{h} wx - \dfrac{q_a x}{h\varepsilon\varepsilon_0} \displaystyle\int_{-\frac{h}{2}}^{\frac{h}{2}} \rho_q dy = \dfrac{d}{dt}(\rho_m whx\bar{u}) \\ -\dfrac{q_a \bar{\lambda}}{\varepsilon\varepsilon_0} + \bar{u}w \displaystyle\int_{-\frac{h}{2}}^{\frac{h}{2}} \left(\frac{3}{2} - 6\frac{y^2}{h^2}\right) \rho_q dy = \dfrac{d}{dt} q_a \end{cases} \tag{27}$$

2.3 Asymptotic solutions

The system of non-linear ordinary differential equations (ODE) Eq. (27) cannot be solved analytically. However, an asymptotic solution can be found. Introducing $\bar{u} = \dot{x}$, $\chi = x\dot{x}$ and $\xi = q_a x/w$

With

$$\hat{F}_s = 2\sigma\cos\theta,$$

$$A = \frac{12\mu}{h},$$

$$B = \frac{1}{h\varepsilon\varepsilon_0} \int_{-\frac{h}{2}}^{\frac{h}{2}} \rho_q dy = \frac{2\zeta\kappa}{h} \tanh\left(\frac{\kappa h}{2}\right),$$

$$C = \rho_m h,$$

$$D = \frac{\bar{\lambda}}{\varepsilon\varepsilon_0}$$

and

$$E = -\varepsilon\varepsilon_0 \zeta\kappa^2 \int_{-\frac{h}{2}}^{\frac{h}{2}} \left(\frac{3}{2} - 6\frac{y^2}{h^2}\right) \frac{\cosh(\kappa y)}{\cosh(\kappa h/2)} dy = \frac{12\varepsilon\varepsilon_0\zeta[\kappa h - 2\tanh(\kappa h/2)]}{(\kappa h)^2},$$

the equation system Eq. (27) can be written as

$$\begin{cases} \hat{F}_s - A\chi - B\xi = C\dot{\chi} \\ -D\xi + E\chi + \frac{\xi}{\chi}\bar{u}^2 = \dot{\xi} \\ (\dot{\chi} - \bar{u}^2)\frac{\bar{u}}{\chi} = \dot{\bar{u}} \end{cases} \tag{28}$$

Apply algebraic transformation

$$\begin{cases} \dot{\chi} = \frac{\hat{F}_s}{C} - \frac{A}{C}\chi - \frac{B}{C}\xi \\ \dot{\xi} = -D\xi + E\chi + \frac{\xi}{\chi}\bar{u}^2 \\ \dot{\bar{u}} = \left(\frac{\hat{F}_s}{C} - \frac{A}{C}\chi - \frac{B}{C}\xi\right)\frac{\bar{u}}{\chi} - \frac{\bar{u}^3}{\chi} \end{cases} \tag{29}$$

By setting $\dot{\chi} = 0$, $\dot{\xi} = 0$, $\dot{\bar{u}} = 0$, it is straightforward to find the solution of Eq. (29) as

$$\begin{cases} \chi = \frac{D\hat{F}_s}{BE+AD} \\ \xi = \frac{E\hat{F}_s}{BE+AD} \\ \bar{u} = 0 \end{cases} \tag{30}$$

Because the velocity approaches zero $\bar{u} \to 0$ when the time goes to infinity $t \to \infty$, the critical point described by Eq. (30) is a stable point. Details of mathematical derivation is shown in Appendix 1. Substituting $\chi = x\dot{x}$ back in to the first equation of Eq. (30) and performing the integration with the initial condition $x(0) = 0$ result in the position of the meniscus as function of time

$$x = \left[\frac{2D\hat{F}_s}{BE + AD} t\right]^{1/2} \tag{31}$$

3 Results and discussion

Equation (31) presents asymptotic solution of the displacement as $t \to \infty$ with consideration of electrokinetic effects. This equation is qualitatively similar to Washburn equation, which stated that $x \propto t^{1/2}$, and therefore, $\bar{u} = \dot{x} \propto t^{-1/2}$. The results lead to a singularity that $\bar{u} \to \infty$when $t \to 0$. However, this singularity is solved with consideration of entrance effect at the initial stage of filling, as discussed in recent studies (Chakraborty 2007; Chakraborty and Mittal 2007; Huang et al. 2001; Chakraborty 2005). In this investigation, as the asymptotic solution is considered, the Eq. (31) is acceptable.

For comparison, the asymptotic solution of the displacement without EDL effect can be expressed as

$$x = \left[\frac{2\hat{F}_s}{A}t\right]^{1/2} \tag{32}$$

Substituting back $\hat{F}_s = 2\sigma\cos\theta$ and $A = 12\ \mu$/h into the two solutions results in

$$\left[\frac{2D\hat{F}_s}{\mathrm{BE}+\mathrm{AD}}t\right]^{1/2} = \left[\frac{\sigma\cos\theta h}{3\mu_a}t\right]^{1/2} \tag{33}$$

$$\left[\frac{2\hat{F}_s}{A}t\right]^{1/2} = \left[\frac{\sigma\cos\theta h}{3\mu}t\right]^{1/2} \tag{34}$$

where μ_a is the apparent viscosity which is higher than the real viscosity μ due to the electrokinetic effects. The ratio between these two viscosities can be obtained as

$$\frac{\mu_a}{\mu} = \frac{\mathrm{BE}+\mathrm{AD}}{2D\hat{F}_s}\frac{2\hat{F}_s}{A} = \left(1+\frac{\mathrm{BE}}{\mathrm{AD}}\right) \tag{35}$$

The relative change of the viscosity can be expressed as

$$\frac{\Delta\mu}{\mu} = \frac{\mu_a-\mu}{\mu} = \frac{\mathrm{BE}}{\mathrm{AD}} = \eta\frac{\tanh\left(\frac{\kappa h}{2}\right)\left[\kappa h - 2\tanh\left(\frac{\kappa h}{2}\right)\right]}{\left[1+\frac{\zeta e}{kT}\frac{v_- - v_+}{v_- + v_+}\frac{2\tanh(\kappa h/2)}{\kappa h}\right](\kappa h)^2} \tag{36}$$

where $\eta = (4\varepsilon\varepsilon_0 N_A\zeta^2 e^2/\mu\Lambda_m kT) \approx (2\varepsilon^2\varepsilon_0^2\zeta^2\kappa^2/\mu\bar{\lambda})$ is a dimensionless parameter.

Under normal conditions, i.e. $\zeta < 100$ mV, $T \approx 300$ K, the dimensionless parameter $\zeta e/kT$ has a value on the order of unity one. For many common binary solutions, where the mobility of ion species is the same, the ratio $\frac{v_- - v_+}{v_- + v_+}$ reduces to zero. In extreme cases, $-1 < \frac{v_- - v_+}{v_- + v_+} < 1$. This ratio does not change the trend of the $\Delta\mu/\mu$ vs. κh significantly, as illustrated in Fig. 3. Therefore, Eq. (36) can be approximated by

$$\frac{\Delta\mu}{\mu} = \eta\frac{\tanh\left(\frac{\kappa h}{2}\right)\left[\kappa h - 2\tanh\left(\frac{\kappa h}{2}\right)\right]}{(\kappa h)^2} \tag{37}$$

The dimensionless channel height κh is determined by both the channel height and the electrolyte concentration.

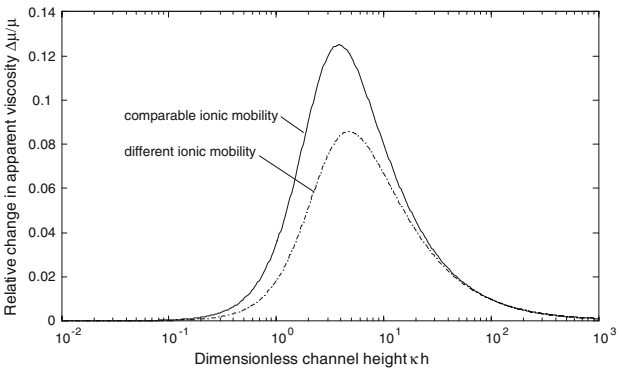

Fig. 3 Dependence of the ratio $\Delta\mu/\mu$ on the dimensionless channel height κh for two different cases (*Dashed line*: mobility of two species of ion is almost the same; *Solid line*: mobility of anion is much higher than that of cation)

At room temperature, Debye length κ^{-1} ranges from several nanometers to a theoretical maximum of submicron for pure water. Therefore, in order to observe electroviscous effect, it is necessary to fabricate channels with height in nanoscale. With a specific channel height, there is one optimum concentration at which the electroviscous effect is most significant. Dilute or concentrate solution (relative to such optimum concentration) gives a lower increase in viscosity, as illustrated in Fig. 4. Figure 5 shows that if the channel height is on the order of tens to hundreds of nanometers, the solution must be very dilute (i.e. 10^{-6} M) to reach the maximum apparent viscosity. At a higher concentration, the viscosity simply increases with the decrease in channel height.

Setting the first order derivative of the relative change of viscosity Eq. (37) to zero shows that the maximum of $\frac{\Delta\mu}{\mu}$ is reached when $\kappa h \approx 4$. Figure 6 shows the ratio $\frac{\Delta\mu}{\mu}$ with respect to normalized channel height κh for various values of η. In Fig. 7, the ratio $\frac{\Delta\mu}{\mu\eta}$with respect to normalized channel height κh is plotted in comparison with corresponding ratio reported previously (Mortensen and

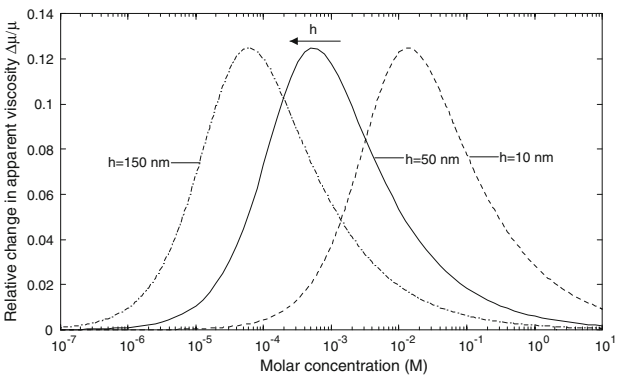

Fig. 4 Ratio $\Delta\mu/\mu$ versus concentration at different channel heights

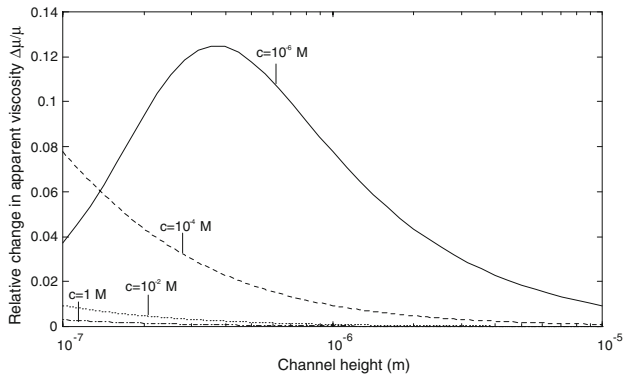

Fig. 5 Ratio $\Delta\mu/\mu$ versus channel height at different concentrations

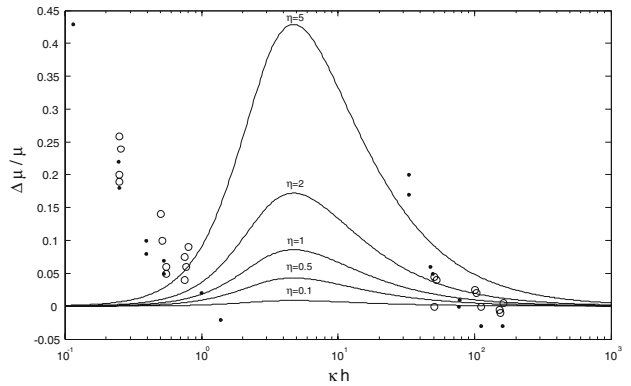

Fig. 6 Ratio $\Delta\mu/\mu$ versus normalized channel height with different η. The *white circles* show experimental results from (Tas et al. 2004). The *black dots* show experimental results from (Persson et al. 2007)

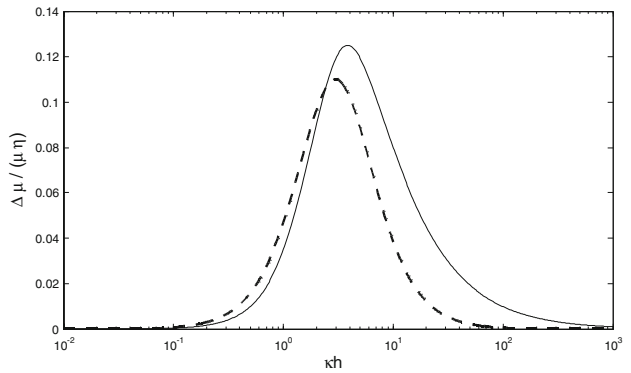

Fig. 7 Ratio $\Delta\mu/(\mu\eta)$ versus normalized channel height. The *solid line* shows results derived from equation (47). The *dashed line* shows corresponding results from Mortensen and Kristensen (2008)

Kristensen 2008), the results showed quite close agreement.

However, the apparent viscosity observed in reported experiments still seems to be higher than that predicted by the present model, as shown in Fig. 5. The deviation between current theories on electroviscous effect and experimental results on the reduction in filling speed suggests that the electroviscous is not the only cause of the speed reduction. There are reports on the formation of air bubbles during the filling process (Han et al. 2006; Thamdrup et al. 2007). The negative pressure across the meniscus in nanochannel may release the gas diluted in the fluid in form of bubbles. A fraction of energy is stored in term of surface energy of the air bubbles; hence, less energy transfers to kinetic energy of the fluid column, which leads to reduction in filling speed. Therefore, in order to observe the electroviscous effect, it is essential to eliminate, or quantitative evaluate other factors contribute in filling speed reduction, such as bubbles formation.

In published literature, many theories have been developed to explain the electroviscous effect in capillary filling. Each approach shown to be convenient in some specific cases. Generally, electroviscous effect is the coupling between electrokinetic and dynamic flow of fluid in the nanochannel. In this investigation, the authors attempted to explain what happens during capillary filling process in a general perspective, to determine which phenomena involve in the filling process, and to represent those phenomena in term of the parameters of final equation. For the sake of readability, simplified models were used to describe these phenomena. However, this approach is also applicable for more complicated cases, which merely lead to the modification of the parameters $\hat{F}_S$, A, B, C, D, and E, without the necessity to rebuild the whole derivation. For each specific case, those parameters can be obtained analytically, numerically, or even experimentally.

4 Conclusions

In conclusion, we have developed a mathematical model for capillary filling in nanochannels. The model describes the electroviscous effects on such capillary filling process. The asymptotic solution showed that the filling process follows Washburn's equation $x \propto \sqrt{t}$, with increasing apparent viscosity. The apparent viscosity is the largest when the dimensionless channel height, namely the ratio between channel height and the Debye length κ^{-1} reaches an optimum value of about 4. A typical Debye length theoretically has values ranging from several nanometers to submicron. Thus, for a dominant electroviscous effect, it is necessary to reduce and precisely control the channel height. The apparent viscosity increases with high zeta potential and low molar conductivity or low ion mobility. Because of the electrostatic interactions during the filling process, the speed of each individual ion/molecule depends on its electric charge and mobility. This phenomenon can be applied to separate different ion species, especially for

those with high molecular weights such as DNAs, polymers or proteins. Further studies can involve the feasibility of chromatography applications.

Appendix 1

To analyze the stability of the critical point found in Eq. (30), it is necessary to rewrite equation Eq. (29) as below

$$\begin{cases} \dot{\chi} = \alpha(\chi,\xi,\bar{u}) = \frac{\hat{F}_s}{C} - \frac{A}{C}\chi - \frac{B}{C}\xi \\ \dot{\xi} = \beta(\chi,\xi,\bar{u}) = -D\xi + E\chi + \frac{\xi}{\chi}\bar{u}^2 \\ \dot{\bar{u}} = \gamma(\chi,\xi,\bar{u}) = \left(\frac{\hat{F}_s}{C} - \frac{A}{C}\chi - \frac{B}{C}\xi\right)\frac{\bar{u}}{\chi} - \frac{\bar{u}^3}{\chi} \end{cases} \tag{38}$$

These non-linear equations cannot be linearized because γ_x, γ_ξ, $\gamma_{\bar{u}}$ reduce to 0 when $\bar{u} = 0$.

However, the stability still can be discovered by considering some experimental facts. First, the capillary filling length x increases with time. Therefore, $\bar{u} = \dot{x}$ is a non-negative function. Second, the viscous force is proportional to $\bar{u}x$. Because the surface tension, as the capillary filling driving force, is a constant, the viscous force must be bound. Therefore, the average velocity $\bar{u}$ must approach 0 when $t \to \infty$. So, the problem reduces to determining the stability of the critical point in $\bar{u} = 0$ hyperplane. With this condition, the Eq. (38) can be rewritten as.

$$\begin{cases} \alpha(\chi,\xi,0) = \frac{\hat{F}_s}{C} - \frac{A}{C}\chi - \frac{B}{C}\xi \\ \beta(\chi,\xi,0) = -D\xi + E\chi \end{cases} \tag{39}$$

To linearize this equation in $\bar{u} = 0$ hyperplane, at the critical point, the Jacobian matrix J is evaluated at that point.

$$J = \begin{bmatrix} \alpha_\chi & \alpha_\xi \\ \beta_\chi & \beta_\xi \end{bmatrix} = \begin{bmatrix} -\frac{A}{C} & -\frac{B}{C} \\ E & -D \end{bmatrix} \tag{40}$$

The eigenvalues λ are calculated by

$$\begin{vmatrix} -\frac{A}{C} - \lambda & -\frac{B}{C} \\ E & -D - \lambda \end{vmatrix} = \left(-\frac{A}{C} - \lambda\right)(-D - \lambda) + \frac{\mathrm{BE}}{C} = 0 \tag{41}$$

Expand the variable

$$\lambda^2 + \left(\frac{A}{C} + D\right)\lambda + \frac{\mathrm{AD} + \mathrm{BE}}{C} = 0 \tag{42}$$

Discriminant Δ

$$\begin{aligned} \Delta &= \left(\frac{A}{C} + D\right)^2 - 4\frac{\mathrm{AD} + \mathrm{BE}}{C} \\ &= \frac{A^2}{C^2} - 2\frac{\mathrm{AD}}{C} + D^2 - \frac{4\mathrm{BE}}{C} \\ &= \left(\frac{A}{C} - D\right)^2 - \frac{4\mathrm{BE}}{C} \end{aligned} \tag{43}$$

It is necessary to know the sign of the reduced variables. By their definition, the variables A, C and D are positive. Both variables B and E are opposite in sign to ζ; therefore, the product BE is positive.

As a result, if $\Delta \geq 0$, two eigenvalues are

$$\lambda_1 = \frac{1}{2}\left(-\frac{A}{C} - D - \sqrt{\Delta}\right) \tag{44}$$

$$\lambda_1 = \frac{1}{2}\left(-\frac{A}{C} - D + \sqrt{\Delta}\right) \tag{45}$$

With A, C and D are positive, λ_1 is negative obviously. In quadratic equation (42)

$$\lambda_1\lambda_2 = 4\frac{\mathrm{AD} + \mathrm{BE}}{C} > 0 \tag{46}$$

Then, λ_2 is also negative. The critical point is a nodal sink (stable).

If $\Delta < 0$, two eigenvalues are complex numbers, with the real parts are

$$\mathrm{Re}(\lambda_1) = \mathrm{Re}(\lambda_2) = \frac{-A - D}{2C} < 0 \tag{47}$$

The critical point is a spiral sink (stable).

Because there is only one finite critical point, and three variables χ, ξ, and $\bar{u}$are bound as $t \to \infty$, the critical point as in Eq. (30) describes the asymptotic solution of the system.

References

Bowen WR, Jenner F (1995) Dynamic ultrafiltration model for charged colloidal dispersions: a Wigner-Seitz cell approach. Chem Eng Sci 50:1707–1736

Burgreen D, Nakache FR (1964) Electrokinetic flow in ultrafine capillary slits. J Phys Chem 68:1084–1091

Chakraborty S (2005) Dynamics of capillary flow of blood into a microfluidic channel. Lab Chip Miniat Chem Biol 5:421–430

Chakraborty S (2007) Electroosmotically driven capillary transport of typical non-Newtonian biofluids in rectangular microchannels. Anal Chim Acta 605:175–184

Chakraborty S (2008a) Generalization of interfacial electrohydrodynamics in the presence of hydrophobic interactions in narrow fluidic confinements. Phys Rev Lett 100

Chakraborty S (2008b) Order parameter description of electrochemical-hydrodynamic interactions in nanochannels. Phys Rev Lett 101

Chakraborty D, Chakraborty S (2008) Interfacial phenomena and dynamic contact angle modulation in microcapillary flows subjected to electroosmotic actuation. Langmuir 24:9449–9459

Chakraborty S, Das S (2008) Streaming-field-induced convective transport and its influence on the electroviscous effects in narrow fluidic confinement beyond the Debye-Hu?ckel limit. Phys Rev E Stat Nonlinear Soft Matter Phys 77

Chakraborty S, Mittal R (2007) Droplet dynamics in a microchannel subjected to electrocapillary actuation. J Appl Phys, 101

Conlisk AT (2005) The Debye-Hu?ckel approximation: its use in describing electroosmotic flow in micro- and nanochannels. Electrophoresis 26:1896–1912

Debye P, Hückel E (1923) The theory of electrolytes. I: lowering of freezing point and related phenomena. Physikalische Zeitschrift 185–206

Eijkel JCT, van den Berg A (2005) Nanofluidics: what is it and what can we expect from it? Microfluid Nanofluid 1:249–267

Han A, Mondin G, Hegelbach NG, de Rooij NF, Staufer U (2006) Filling kinetics of liquids in nanochannels as narrow as 27 nm by capillary force. J Colloid Interface Sci 293:151–157

Hsu JP, Kao CY, Tseng S, Chen CJ (2002) Electrokinetic flow through an elliptical microchannel: effects of aspect ratio and electrical boundary conditions. J Colloid Interface Sci 248:176–184

Huang KD, Yang RJ (2007) Electrokinetic behaviour of overlapped electric double layers in nanofluidic channels. Nanotechnology 18

Huang KD, Yang RJ (2008) Formation of ionic depletion/enrichment zones in a hybrid micro-/nano-channel. Microfluid Nanofluid 1–8

Huang W, Bhullar RS, Yuan Cheng F (2001) The surface-tension-driven flow of blood from a droplet into a capillary tube. J Biomech Eng 123:446–454

Huang W, Liu Q, Li Y (2006) Capillary filling flows inside patterned-surface microchannels. Chem Eng Technol 29:716–723

Hunter RJ (1981) Zeta potential in colloid science: principles and applications. Academic Press

Jeong HE, Kim P, Kwak MK, Seo CH, Suh KY (2007) Capillary kinetics of water in homogeneous, hydrophilic polymeric micro- to nanochannels. Small 3:778–782

Kundu PK, Cohen IM (1990) Fluid mechanics. Academic Press

Lerch MA, Jacobson SC (2007) Electrokinetic fluid control in two-dimensional planar microfluidic devices. Anal Chem 79:7485–7491

Levine S, Neale GH (1974) The prediction of electrokinetic phenomena within multiparticle systems. I: electrophoresis and electroosmosis. J Colloid Interface Sci 47:520–529

Levine S, Marriott JR, Neale G, Epstein N (1975a) Theory of electrokinetic flow in fine cylindrical capillaries at high zeta-potentials. J Colloid Interface Sci 52:136–149

Levine S, Marriott JR, Robinson K (1975b) Theory of electrokinetic flow in a narrow parallel-plate channel. J Chem Soc Faraday Trans 2 Mol Chem Phys 71:1–11

Lyklema J, van Leeuwen HP, Vliet M, Cazabat A-M (2005) Fundamentals of interface and colloid science. Academic Press

Mijatovic D, Eijkel JCT, van den Berg A (2005) Technologies for nanofluidic systems: Top-down vs. bottom-up—a review. Lab Chip Miniat Chem Biol 5:492–500

Mohiuddin Mala G, LI D (1999) Flow characteristics of water in microtubes. Int J Heat Fluid Flow 20:142–148

Mortensen NA, Kristensen A (2008) Electroviscous effects in capillary filling of nanochannels. Appl Phys Lett 92

Mortensen NA, Diesen LH, Bruus H (2006) Transport coefficients for electrolytes in arbitrarily shaped nano- and microfluidic channels. New J Phys 8

Mortensen NA, Olesen LH, Okkels F, Bruus H (2007) Mass and charge transport in micro and nanofluidic channels. Nanoscale Microscale Thermophys Eng 11:57–69

Nguyen N-T (2008) Micromixers fundamentals, design and fabrication. William Andrew

Perry JL, Kandlikar SG (2006) Review of fabrication of nanochannels for single phase liquid flow. Microfluid Nanofluid 2:185–193

Persson F, Thamdrup LH, Mikkelsen MBL, Jaarlgard SE, Skafte-Pedersen P, Bruus H, Kristensen A (2007) Double thermal oxidation scheme for the fabrication of SiO_2 nanochannels. Nanotechnology 18:246301

Petsev DN (2008) Transport in fluidic nanochannels. Colloidal Background, Nanoscience

Philip JR, Wooding RA (1970) Solution of the poisson-Boltzmann equation about a cylindrical particle. J Chem Phys 52:953–959

Ren CL, Li D (2005) Improved understanding of the effect of electrical double layer on pressure-driven flow in microchannels. Anal Chim Acta 531:15–23

Reuss FF (1809) Sur un nouvel effet de l'electricite galvanique. Memoires de la Societe Imperiale de Naturalistes de Moscou

Rice, Whitehead (1965) Electrokinetic flow in a narrow cylindrical capillary. J Phys Chem 69:4017–4023

Russel WB, Saville DA, Schowalter WR (1989) Colloidal dispersions, Cambridge University Press

Sherma J (2002) Planar chromatography. Anal Chem 74:2653–2662

Sherma J (2004) Planar chromatography. Anal Chem 76:3251–3262

Sherma J (2006) Planar chromatography. Anal Chem 78:3841–3852

Sherma J (2008) Planar chromatography. Anal Chem 80:4253–4267

Smoluchowski (1903) Contribution a la theorie de l'endosmose electrique et de quelques phenomenes correlatifs. Bulletin International de l'Academie des Sciences de Cracovie 182–200

Tas NR, Mela P, Kramer T, Berenschot JW, van den Berg A (2003) Capillarity induced negative pressure of water plugs in nanochannels. Nano Lett 3:1537–1540

Tas NR, Haneveld J, Jansen HV, Elwenspoek M, van den Berg A (2004) Capillary filling speed of water in nanochannels. Appl Phys Lett 85:3274–3276

Tas NR, Haneveld J, Jansen HV, Elwenspoek M, Brunets N (2008) Capillary filling of sub-10 nm nanochannels. J Appl Phys 104:014309

Thamdrup LH, Persson F, Bruus H, Kristensen A, Flyvbjerg H (2007) Experimental investigation of bubble formation during capillary filling of SiO_2 nanoslits. Appl Phys Lett 91

van Delft KM, Eijkel JCT, Mijatovic D, Druzhinina TS, Rathgen H, Tas NR, van den Berg A, Mugele F (2007) Micromachined fabry-perot interferometer with embedded nanochannels for nanoscale fluid dynamics. Nano Lett 7:345–350

van Honschoten JW, Escalante M, Tas NR, Jansen HV, Elwenspoek M (2007) Elastocapillary filling of deformable nanochannels. J Appl Phys 101

Verwey EJW, Overbeek JTG (1948) Theory and stability of lyophobic colloids. Elsevier, Amsterdam

Washburn EW (1921) The dynamics of capillary flow. Phys Rev 17:273

Yang C, LI D (1997) Electrokinetic effects on pressure-driven liquid flows in rectangular microchannels. J Colloid Interface Sci 194:95–107

Yang J, Lu F, Kwok DY (2004) Dynamic interfacial effect of electroosmotic slip flow with a moving capillary front in hydrophobic circular microchannels. J Chem Phys 121:7443–7448

Yuan Z, Garcia AL, Lopez GP, Petsev DN (2007) Electrokinetic transport and separations in fluidic nanochannels. Electrophoresis 28:595–610

Zimmermann M, Schmid H, Hunziker P, Delamarche E (2007) Capillary pumps for autonomous capillary systems. Lab Chip Miniat Chem Biol 7:119–125